Bilayer Graphene Grown on 4H-SiC (0001) Step-Free Mesas

ARTICLE *in* NANO LETTERS · MARCH 2012

Impact Factor: 13.59 · DOI: 10.1021/nl203353f · Source: PubMed

NANO LETTERS

Letter

pubs.acs.org/NanoLett

Bilayer Graphene Grown on 4H-SiC (0001) Step-Free Mesas

L.O. Nyakiti,* R. L. Myers-Ward, V. D. Wheeler, E. A. Imhoff, F.J. Bezares, H. Chun, J. D. Caldwell, A. L. Friedman, B. R. Matis, J. W. Baldwin, P. M. Campbell, J. C. Culbertson, C. R. Eddy, Jr., G. G. Jernigan, and D. K. Gaskill

U.S. Naval Research Laboratory, 4555 Overlook Avenue SW, Washington, D.C. 20375, United States

Supporting Information

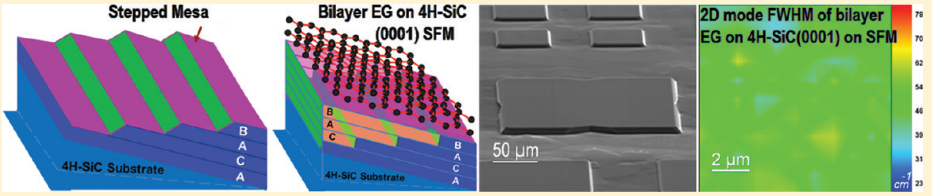

ABSTRACT: We demonstrate the first successful growth of large-area (200 × 200 μm^2) bilayer, Bernal stacked, epitaxial graphene (EG) on atomically flat, 4H-SiC (0001) step-free mesas (SFMs) . The use of SFMs for the growth of graphene resulted in the complete elimination of surface step-bunching typically found after EG growth on conventional nominally on-axis SiC (0001) substrates. As a result heights of EG surface features are reduced by at least a factor of 50 from the heights found on conventional substrates. Evaluation of the EG across the SFM using the Raman 2D mode indicates Bernal stacking with low and uniform compressive lattice strain of only 0.05%. The uniformity of this strain is significantly improved, which is about 13-fold decrease of strain found for EG grown on conventional nominally on-axis substrates. The magnitude of the strain approaches values for stress-free exfoliated graphene flakes. Hall transport measurements on large area bilayer samples taken as a function of temperature from 4.3 to 300 K revealed an n-type carrier mobility that increased from 1170 to 1730 $cm^2\ V^{-1}\ s^{-1}$, and a corresponding sheet carrier density that decreased from 5.0 × 10^{12} cm^{-2} to 3.26 × 10^{12} cm^{-2}. The transport is believed to occur predominantly through the top EG layer with the bottom layer screening the top layer from the substrate. These results demonstrate that EG synthesized on large area, perfectly flat on-axis mesa surfaces can be used to produce Bernal-stacked bilayer EG having excellent uniformity and reduced strain and provides the perfect opportunity for significant advancement of epitaxial graphene electronics technology.

KEYWORDS: *Bilayer epitaxial graphene, step-free SiC mesa, Raman 2D mode, lattice strain, charge transport*

Epitaxial graphene (EG) has many exciting material properties that promise advancements in electronics,[1,2] specifically in the fabrication of RF field-effect transistors.[3] Several groups have reported EG growth with high carrier mobilities at room temperature[4−7] utilizing Si sublimation of α-SiC substrates (where α can either be the 4H or 6H polytype). Although EG has been formed on α-SiC(0001) substrates up to 76.2 mm in diameter,[3,4] the presence of surface morphological inhomogeneities[8,9] and lattice strains[10] are reported to degrade electrical properties,[6,7,11−13] which consequently limit the performance of fabricated devices. For example, EG growth on α-SiC(0001) results in step-bunching of the underlying substrate with vertical step heights of ∼5−15 nm.[8−10,14−16] Step-bunching poses a significant challenge to graphene device development, for instance, Yakes et al.[17] demonstrated an increased electrical resistance of EG over the step bunch. And, Lin et al.[14] observed increased resistance for graphene device channels placed across the step-bunched edge. The increased electrical resistance in both studies necessitates the fabrication of device structures on irregularly spaced, narrow terrace widths (typically ∼2−5 μm wide) that presents a significant processing challenge. It is therefore desirable to form graphene over large areas with minimal strain and no step-bunching. Single layer graphene does not have a band gap, which is needed to improve the overall on/off performance of graphene-based electronic devices, and so there is also great interest in controllably forming Bernal stacked (AB) bilayer graphene, since it has been shown to have a band gap when subjected to an electric field.[18−21] In this work, we report for the first time the growth of Bernal stacked (AB) bilayer epitaxial graphene on atomically flat 4H-SiC (0001) homoepitaxial layers on patterned substrate mesas, heretofore referred to here as step-free mesas (SFMs). The growth resulted in the complete elimination of step-bunching widely prevalent for EG grown on conventional nominally on-axis 4H-SiC (0001) substrates that is known to impact electronic device performance. The EG formed on SFMs also has low, uniform strain approaching that of exfoliated samples which is a significant improvement over what is observed for EG grown on conventional substrates. Hall Effect measurements on EG grown on SFM show electrical

Received: June 26, 2011
Revised: December 28, 2011
Published: February 21, 2012

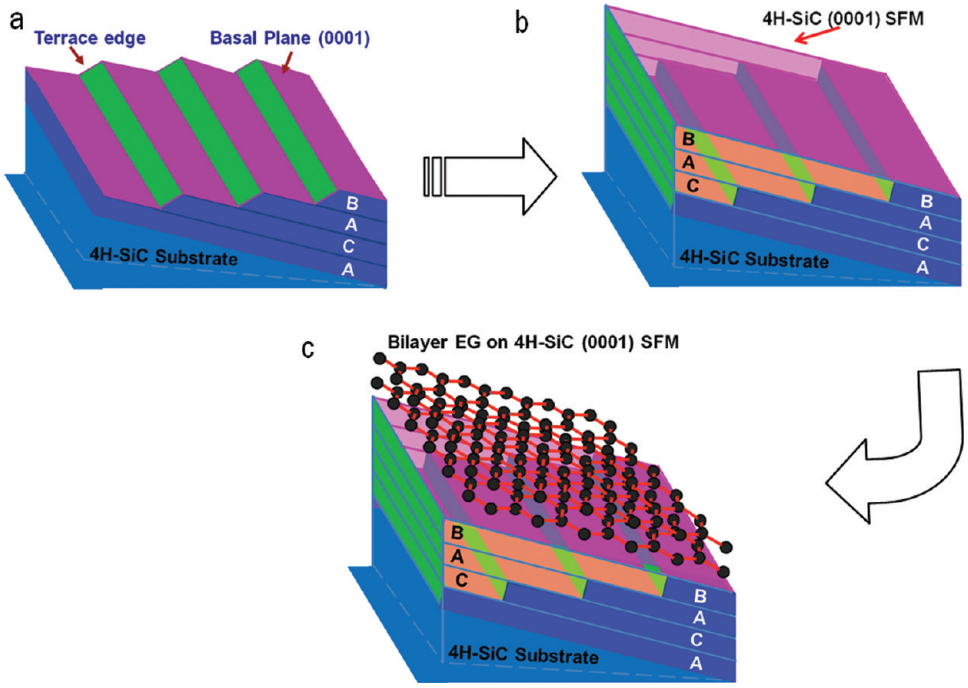

Figure 1. Schematic depiction of surface morphology of (a) a patterned stepped mesa after H_2 etch and prior to homoepitaxial growth of n-doped 4H-SiC. (b) Step-free mesa after homoepitaxial growth of the steps to the mesa edge that replicates the underlying tetrahedrally bonded Si−C bilayer stacking sequence of "ACAB..." and forming an atomically smooth 4H-SiC surface and (c) bilayer EG formation on a SFM.

properties over very large areas (>10^4 μm^2) comparable to results found for smaller area exfoliated bilayer samples and demonstrate the high quality of these films.

Neudeck et al.[22,23] and others[24,25] reported that the lateral homoepitaxy of 4H-SiC on nearly on-axis (<0.5° off-cut) 4H-SiC mesas lacking screw dislocations produces atomically flat step-free surfaces. The step-free mesa surface forms a perfect stacking sequence of atomic bilayers of Si−C for the bilayer EG growth via the process depicted in Figure 1. Fabrication of quarters of 76.2 mm weakly conducting SiC substrates (Cree Inc.) that are nominally on-axis (0.25° off-cut) into SFMs followed by graphene growth involves multiple process steps. Standard photolithography and ICP-RIE using a metal mask was used to pattern the wafer surface into square and hexagonal mesas with side lengths ranging from 40 to 200 μm and vertical height of 2 μm. Subsequent kinetically controlled step-flow homoepitaxial growth[24] of lightly n-doped 4H-SiC, depicted in Figure 1b, was conducted in a commercial Aixtron/Epigress hot-wall chemical vapor deposition reactor. (Details about SFMs formation can be found in Supporting Information.) In principle, the growth of SFMs can be extended to much larger-sized mesas since the limiting factor is that the growth area cannot contain a screw dislocation, which will source surface steps. The source of screw dislocations is the substrate, and in state-of-the-art SiC wafers the density of screw dislocations is $\leq 1.0 \times 10^3 cm^{-2}$ [26] and, thus, mesas with side lengths ~350 μm should be possible.

Following homoepitaxial growth of SFMs, the quarter wafers were diced into ~16 mm squares before EG synthesis. Growth of bilayer epitaxial graphene was realized by Si sublimation at 1620 °C under a 100 mbar argon environment for a total of 2.5 h using the approach described by Tedesco et al.[9] The growth times used on the SFMs reported here are comparable to growth times of bilayer graphene on nominally on-axis 4H-SiC (conventional) substrates using similar growth conditions. To compare the unique properties of EG grown on SFMs to that of EG grown on conventional substrates, a second set of 16 mm square EG samples were simultaneously synthesized as "witness" samples; these samples exhibit step-bunching as has been described previously[9−11,27] (Additional details about EG growth on conventional substrates can be found in the Supporting Information.)

Nomarski differential interference contrast microscopy was used to identify step-free mesas within the samples before graphene formation, as well as to characterize EG morphology afterward. A Veeco scanning probe D3100 atomic force microscope (AFM) operating under ambient conditions in tapping mode (vertical resolution ~0.1 nm) and LEO Supra 55 scanning electron microscope were used to extract surface morphological variations across the samples. The presence, layer thickness, and strain variation across the EG synthesized on the two different types of substrate surfaces were determined by confocal micro-Raman spectroscopy with a spectral resolution of 7 cm^{-1} and using an excitation power, wavelength, and spot size of 150 mW, 514.5 nm, and 0.7 μm, respectively. Maps of parameters obtained from the Raman spectra were constructed using lateral step sizes that varied from 0.4 to 1 μm, depending on the x- and y-directions scan range. Epitaxial graphene that also formed between the mesas was removed before subsequent electrical characterization. A thick masking layer of photoresist was used to protect the graphene on the step-free mesa surfaces and the removal was performed using reactive ion oxygen plasma. Electrical contact was made on the corners of square bilayer EG on SFMs samples by evaporating Ti (5 nm)/Au (45 nm) electrodes in a van der Pauw arrangement defined by electron beam lithography. The corners were designated clockwise as 1, 2, 3, and 4. The devices were cooled in a cryogenic probe station with a base pressure of 1×10^{-8} Torr and base temperature of T ~ 1.7 K. Electrical transport measurements were carried out

dx.doi.org/10.1021/nl203353f | Nano Lett. 2012, 12, 1749−1756

using AC lock-in techniques at a frequency of 13.7 Hz. An excitation current of no more than 100 nA was used to prevent Joule heating. The sheet resistance ρ was obtained with the equation $\rho = [\pi/2\ln(2)][(V_{43}/I_{12}) + (V_{14}/I_{23})]$, where I_{ab} and V_{cd} represent the current source measured between corners a and b and measured voltage drop across corners c and d.

Initial assessments of the mesas were made by Nomarski microscopy to identify SFMs before graphene growth. Figure 2a and the inset show examples of mesas with and without crystalline defects, such as axial threading screw dislocations that would source surface steps. EG growth on defective stepped-mesas, such as those shown in the figure 2a was also evaluated to compare thickness and strain variation relative to SFMs. The morphology of the EG on the SFMs evaluated by Nomarski microscopy were found to be uniform with no discernible imperfections, as can be seen in the Nomarski micrograph shown in Figure 2b. The flatness of EG on the SFMs was confirmed by SEM and electron channeling contrast imaging (not shown).[28]

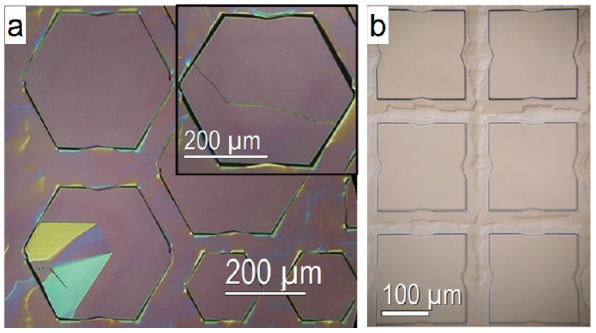

Figure 2. Nomarski optical micrographs of (a) hexagonal mesas after homoepitaxial growth of 4H-SiC with step-free surface (upper left), screw dislocation (lower left), and stepped (inset) structural morphologies, and (b) surface morphology of bilayer EG on square step-free mesas with side lengths ~200 μm.

Figure 3a presents an AFM height-scan image of EG on a SFM. As can be seen in this 100 μm × 100 μm scan, the EG exhibits greatly improved morphology in comparison to conventional substrates, that is, no steps or step-bunching are observed. Precise measurements of surface roughness for SFMs before and after graphene synthesis were limited by AFM instrument resolution at ambient environment, $\leq$ 0.1 nm. The height variations of this morphology are found to be significantly reduced from the step-bunched heights of 5−15 nm typically found after EG growth on conventional α-SiC substrates,[8,9] an example of which is shown in Figure 3b,c, indicating a 50- to 150-fold improvement.

Raman spectroscopy was used to evaluate EG on SFMs through spatial maps of the 2D band position (strain) and full width at half-maximum (fwhm) (thickness)[10,29−36] (Figure 4a−f). Two regions are assessed in detail here, the first at the mesa center and the second near the mesa edge denoted as 1 and 2, respectively, in Figure 4a. Maps for other regions within the center of SFMs can be found in the Supporting Information Figure S1−S4. For region 1, the 2D band fwhm spectral map can be found in Figure 4c. In this case, the 2D band fwhm from several locations from region one were fitted to various number of Lorentzian functions without imposing any constraints and the data was found to be consistent with bilayer graphene, as will be described presently.

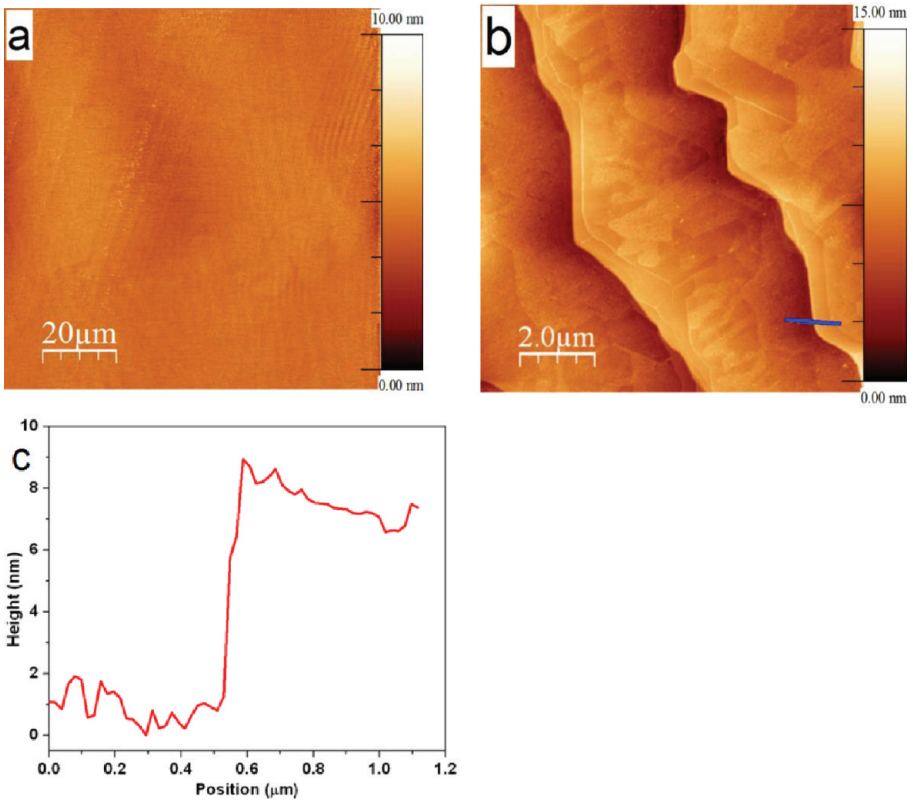

Figure 3. AFM micrographs of EG on SFM for a (a) 100 × 100 μm^2 height scan showing lack of step-bunching, (b) AFM height scan of step-bunched EG on conventional 4H-SiC substrate, showing step-bunching, and (c) line profile of a step-bunch showing a height of ~10 nm.

dx.doi.org/10.1021/nl203353f | Nano Lett. 2012, 12, 1749−1756

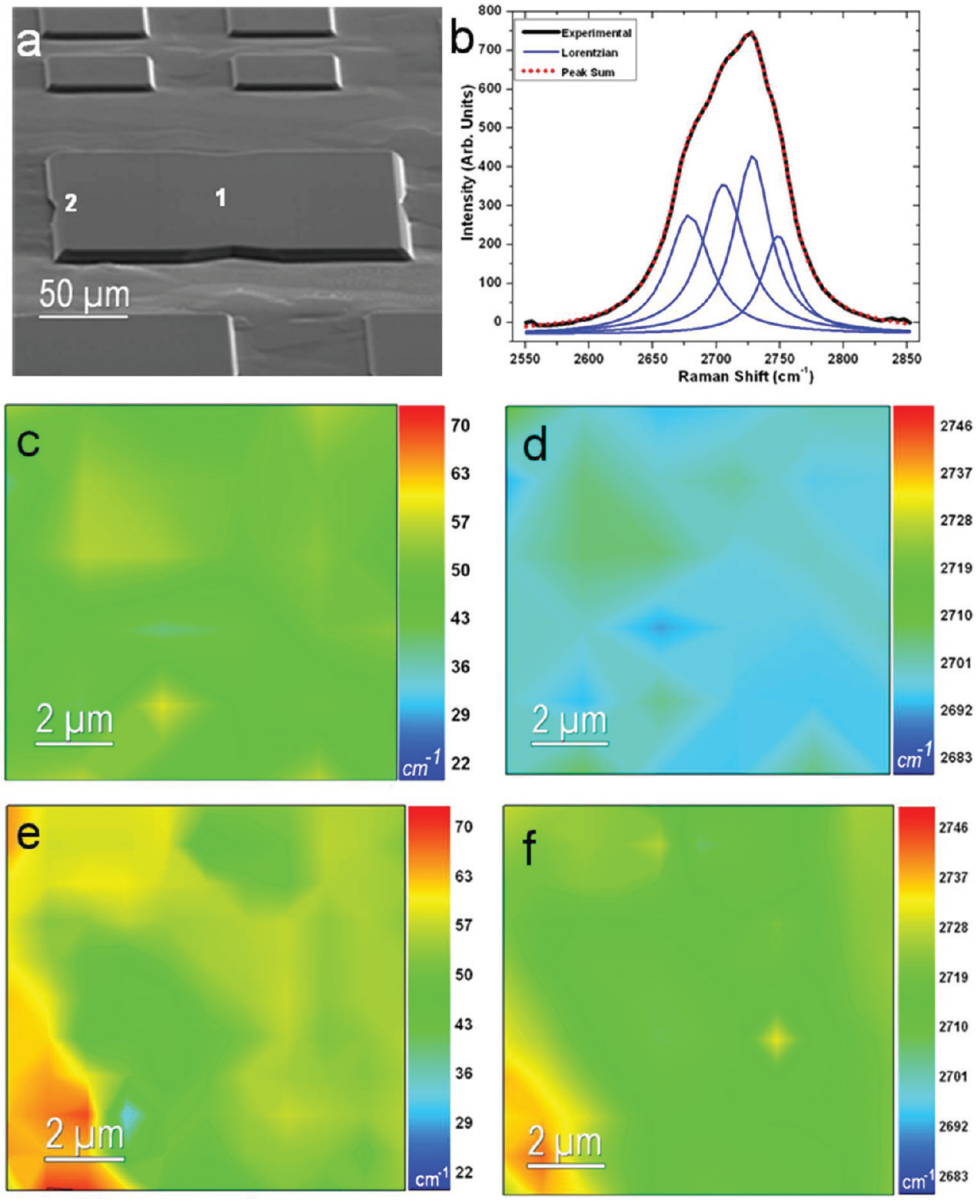

Figure 4. (a) SEM micrograph showing a lack of resolvable structural features of EG that has been synthesized on a SFM with side length of 200 μm, regions 1 and 2 (used in panels c–f) marked. (b) A representative 2D band fitted with a set of four Lorentzian functions confirming presence of Bernal-stacked bilayer EG. (c,d) The 2D fwhm and band position maps from region 1 showing the variation in layer thickness and strain near the mesa edge. (e,f) The 2D fwhm and band position maps from region 2 having bilayer EG; two distinct EG areas are observed: (i) red/orange areas showing onset of multilayer EG, and (ii) green areas representing bilayer EG.

Attempts to fit the EG 2D mode spectra from the center of SFM region 1 by a single Lorentzian function were unsuccessful, as shown in Figure S7 (Supporting Information). The inability to fit one Lorentzian component with the experimental spectrum means that it is not monolayer graphene.[33] In addition, the experimental 2D fwhm, ~60 cm^{-1}, is too large compared to results found by others for a monolayer film, ~25–40 cm^{-1} [36,40] using a similar excitation wavelength, again implying the experimental result is not from a monolayer graphene. Attempts to fit two Lorentzians were also unsuccessful, shown in Supporting Information Figure S8. This means that it is not graphite, which yields two Lorentzian contributions from the AB stacked planes to the 2D mode that typically has a fwhm ~40 cm^{-1}, again much less than experimentally measured here.[33]

Fitting the 2D data to a sum of the four Lorentzian functions converged perfectly to experimental data, shown in Figure 4b. In addition, the positions of the four fit components are consistent with the theoretical predictions for bilayer graphene, see Supporting Information Table S1, where the difference between experiment and theory is mainly due to the resolution of our spectrometer. This implies the sample is Bernal-stacked bilayer EG. The data is also consistent with other reports for bilayer graphene; for example exfoliated bilayer graphene exhibits a 2D fwhm ~50 cm^{-1},[33] and other reports yield a range of 41–60 cm^{-1}.[10,36–39] It is noteworthy that Robinson J. A. et al.[10] successfully used Raman spectroscopy to identify bilayer EG on step-bunched (conventional) SiC(0001) and validated the results by use of high-resolution transmission electron microscopy.

dx.doi.org/10.1021/nl203353f | *Nano Lett.* 2012, 12, 1749–1756

We did not attempt to fit the data to a sum of 6 Lorentzians (required for 3 monolayers of graphene) as a false positive may result. Instead, we note that the 2D fwhm for 3 monolayers is ~70 cm^{-1} for the excitation wavelength used here,[39] larger than experimentally measured. Likewise, for 4 or more layers, even larger fwhm would be exhibited, again not found experimentally found here. Thus, the Raman data presented supports only bilayer graphene in the center of region one. Lastly, we tested a few other locations and found the results were similar, that is the 2D spectra were fit to a sum of four Lorentzians. Given the uniformity of the fwhm in the Raman spatial maps found in Figure 4 c and e, complete Bernal bilayer graphene coverage is implied.

The 2D band fwhm map for region 2 is shown in Figure 4e. The majority of 2D band spectra found in the Figure 4e map can also be fit to a sum of four Lorentzian functions without constraints,[10] indicative of Bernal stacked bilayer graphene, (fwhm from 42 to 60 cm^{-1}). Additional regions of the mesa (not shown) were also tested and, except for locations near the mesa edge, yielded results consistent with Bernal stacked bilayer graphene. For locations where EG was within approximately 2 μm of all the mesa edges, the left-hand-side portion of Figure 4e, the Raman 2D spectra was best fit by two Lorentzian functions, indicating the presence of EG with >2 layers since the fwhm ranged from 61 to 70 cm^{-1}, as graphite would not be possible since the measured fwhm was too large (graphite ~40 cm^{-1}, see above). An example fit with two Lorentzians can be found in the Supporting Information, Figure S5. Lastly, we note the formation of EG bilayer graphene with AB stacking sequence is not surprising, as small areas of bilayer epitaxial graphene on Si face of conventional substrates, typically at step bunches, have been shown to be Bernal stacked.[10] Thus, SFMs promote uniform, large-area Bernal-stacked bilayer graphene formation with small regions of slightly thicker (>2 layers) within 2 μm of the edge of the mesa.

The formation of >2 graphene layers at the mesa edges is attributed to the growth mechanism of EG on SFMs. We base this upon preliminary experiments involving reduced growth time (1.5 h) that produced incomplete EG synthesis on SFMs; an SEM image of this surface is presented in Figure 5. The dark region near the mesa edge in Figure 5 is confirmed to be graphene by Raman spectroscopy (not shown) whereas the central white region lacks any evidence of graphene. The morphology of the graphene "finger" features found near the mesa edge, see Figure 5 inset, are not novel and are similar to those observed by Ohta et al.[42] and Bolen et al.[12] who demonstrated that such features are due to carbon diffusion. This implies that the graphene growth begins at the mesa edge and involves a carbon diffusion mechanism that most likely originates near the mesa edge. Therefore, the thickness mechanism on SFMs is similar in nature to conventional substrates. Hence, we expect the graphene to be thicker at the mesa edge for all growth times, consistent with the graphene thickness results on SFM discussed above and shown in Figure 4. Additional investigations are needed to fully understand the graphene growth kinetics for this unique geometry.

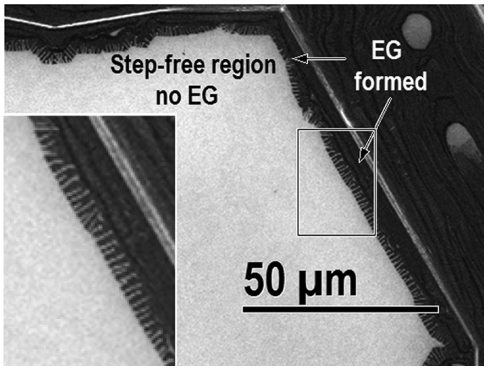

Figure 5. SEM micrograph showing an incomplete EG synthesis (1.5 h shorter growth time) on a SFM. The dark region near the mesa edge has rapid EG formation while the central SFM (white colored region) lacks any evidence of graphene. Magnified image of a boxed region near the SFM edge (inset) illustrates finger formation, implying growth initiation commences at the mesa edge.

The 2D band position variation has been used to directly extract the lattice strain of graphene, whether exfoliated or epitaxial and for monolayer, Bernal bilayer, or turbostratic multilayer graphene.[33−36,44] The magnitude of strain (ε) in bilayer EG can be determined from the shift of the 2D band as measured against unstrained samples using $\varepsilon = -[\Delta\omega_{2D}][0.817\omega'_{2D}\beta_{2D}]^{-1}$, where ε is the strain, $\Delta\omega_{2D}$ is the shift of the peak position from strain-free exfoliated bilayer graphene, ω'_{2D} is the peak position of mechanically exfoliated strain-free bilayer graphene, 2696 cm^{-1}, and $\beta_{2D} = 2.7$ is the Gruneisen parameter for bilayer EG. Additional details can be found in the Supporting Information. Figure 4d,f shows the 2D band position maps for regions 1 and 2, respectively. The 2D band position is observed to remain relatively unchanged over the step-free mesa region as demonstrated in the image, indicating uniform strain across the mesa except near the edge. The 2D band position for region 1 (mesa center) averages ~2699 ± 4.4 cm^{-1} ($\varepsilon = -0.05\%$) and is shifted from the average position for region 2 (mesa edge) ~2726 ± 5.4 cm^{-1} ($\varepsilon = -0.51\%$). This implies that the compressive strain of the graphene near the edge has increased relative to that of the center. The strain measurements from region 1 attain values equivalent to or approaching strain-free mechanically exfoliated Bernal-stacked bilayer graphene (2696 cm^{-1}).[33] Selected locations of the mesa away from the edge (not shown) were also examined and yielded results indicative of minimal strain as found in region 1. Therefore the SFMs enable EG with extremely low and uniform strain.

EG grown on defective mesa surfaces, that is, mesas containing axial threading screw dislocations similar to those observed in Figure 2a, produced a nonuniform 2D fwhm map as shown in Figure 6a, consisting of scattered areas having bilayer and >2 EG layers. Further, the peak positions of the 2D band for the defective stepped mesas, shown in Figure 6b, had an average peak position of the central portion of the mesa of 2712 ± 4.9 cm^{-1} ($\varepsilon = -0.27\%$), which shows the strain is larger than that for EG on SFMs.

Figure 6c,d shows the 2D band fwhm and peak position maps of high quality EG (300 K van der Pauw Hall mobility of 1152 $cm^2\ V^{-1}\ s^{-1}$ and electron carrier density of 8.6×10^{12} cm^{-2}) purposefully grown on conventional 4H-SiC substrates (representative AFM image is shown in Figure 3c) to result in bilayer graphene on the terraces and multilayer at the step edges (determined by fitting the 2D band). The 2D band peak positions had an average value of 2735 ± 3.7 cm^{-1} ($\varepsilon = -0.66\%$) and 2747 ± 5.0 cm^{-1} ($\varepsilon = -0.86\%$), for bilayer and multilayer covered regions, respectively. These higher strain values for EG on a conventional substrate are in agreement with literature results,[29,33,43,45] with ε ranging from −0.3 to

dx.doi.org/10.1021/nl203353f | Nano Lett. 2012, 12, 1749−1756

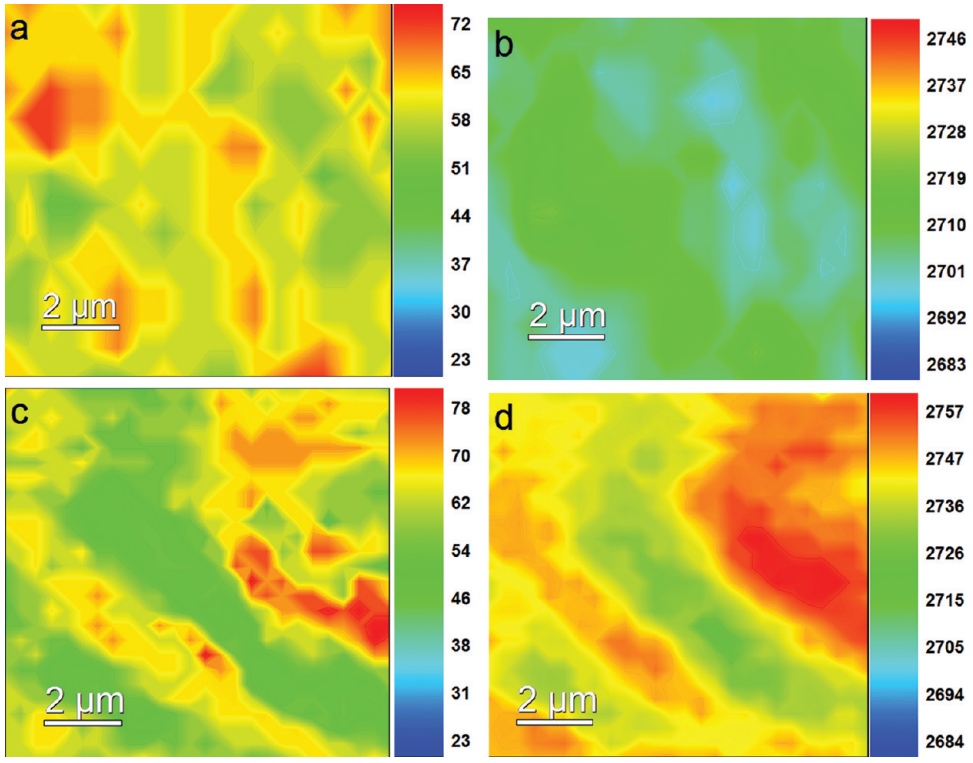

Figure 6. (a,b) The evolution of Raman 2D fwhm and mode position maps of EG synthesized on defective (stepped) mesa due to axial threading screw dislocation. The 2D fwhm map show a bilayer (green) and >2 layers regions (red) while the 2D peak position maps show fairly uniform strain with an average peak position of 2712 ± 4.9 cm^{-1} (ε = −0.27%). (c,d) Nonuniform Raman 2D fwhm and band position maps of EG on a step-bunched nominally on-axis 4H-SiC (0001). The strains varying from ∼2735 ± 3.7 cm^{-1} (ε = −0.66%) to 2747 ± 5.0 cm^{-1} (ε = −0.86%).

−1.17%. The strain values found for EG on conventional substrates are significantly higher (13- to 17-fold increase) than those obtained from graphene grown on SFMs, or even defective mesa surfaces (2 to 3 fold higher), as shown in Figure 4c−f.

The large difference in the coefficients of thermal expansion between EG and SiC has been proposed to give rise to EG compressive strain during cool-down from growth temperatures.[33,36] Yet, EG on SFMs do not exhibit significant strain or strain variations except near the mesa edge. Further, the higher and nonuniform strain values of EG grown on conventional substrates, which possess considerable step-bunching, suggests that EG strain relief is somehow inhibited at step edges. The intermediate value of strain found for EG on defective mesas is consistent with such an inhibition.

The measured sheet resistance for the bilayer graphene material was 1.0 kΩ/□ at 4.3 K and varied less than 10% at 300 K (1.1 kΩ/□). Such a small change in the resistivity across a wide temperature range suggests that any transport gap opening between the two layers of the bilayer graphene device is negligibly small, which is not surprising, given the absence of an applied perpendicular electric field. As an additional measure of clarification, we assessed the electrical properties of the n-type substrate and found the sheet resistance to be much greater than EG (38.7 kΩ/□ at 300 K and 39 kΩ/□ at 4.3 K) and did not contribute significantly to electrical measurements. Further, no conductivity was measured between adjacent mesas since the EG layer had been stripped off by RIE. While there is no graphene connecting the mesas, they should still have been electrically connected by the substrate. However, the data did not bear this out, resistance measurement taken across the two adjacent mesas yielded >1.0 × 10^8 Ω, Additionally, we measured the electrical properties of the n-type substrate and found the mobility to be 11 cm^2 V^{-1} s^{-1} at 300 K and 24 cm^2 V^{-1} s^{-1} at 4.3 K; the lack of transport between EG from SFM-to-SFM implies that the top layer of graphene was insulated from the substrate by the bottom layer of graphene. While there should be no graphene connecting the mesas after this processing step, individual mesas should still have been connected by the conducting substrate. However, electrical measurements indicated that mesas were not electrically connected, which strongly suggests that the top layer of graphene was insulated from the substrate by the bottom layer of graphene. This is perfectly in line with measurements (long known) that show a ∼10^4 Ω-cm conductance anisotropy in stacked graphene layers.[46] It also indicates the high structural quality (step-bunches etc.) of the graphene grown on mesas because there were no electrical shorts caused by edge state conduction.

Since the electrical transport properties of bilayer graphene are significantly different from that of single layer graphene,[41] an initial investigation was carried out. The Hall mobility, μ, of the charge carriers is calculated using $\mu = |R_H|/\rho$, where R_H is the Hall coefficient. A measurement of the Hall coefficient R_H in a field of 0.25 T yielded a mobility of the n-type charge carriers of 1170 cm^2 V^{-1} s^{-1} at 4.3 K with a carrier concentration of 5.08 × 10^{12} cm^{-2}. The mobility was found to increase to 1730 cm^2 V^{-1} s^{-1} at 300 K while the charge carrier density decreased to 3.26 × 10^{12} cm^{-2} at 300 K. The increase in mobility with increasing temperature has been observed previously for bilayer graphene exfoliated flakes[47] (likely Bernal stacked) and our mobility is about a factor of 2 higher for similar carrier density. We believe this work is the first report of electrical properties for Bernal stacked bilayer EG

dx.doi.org/10.1021/nl203353f | Nano Lett. 2012, 12, 1749−1756

on 4H-SiC. As EG formation on SFMs is optimized, it is anticipated that improved electrical properties will be realized. These exciting new results warrant additional in-depth transport investigations, which are underway.

In summary, synthesis of large-area Bernal-stacked bilayer epitaxial graphene on 4H-SiC step-free mesas has been demonstrated for the first time. These engineered surfaces lack any indications of SiC step-bunching before or after EG growth. Most importantly, EG films on step-free mesas demonstrate significantly reduced strain (13×) approaching that of free-standing exfoliated flakes. These results demonstrate that the properties of EG synthesized on SiC without the interference of steps (as such steps are here proposed to inhibit strain relaxation) are closer to those of exfoliated samples. Hall Effect measurements showed an increase in electron carrier mobility from 1170 $cm^2\ V^{-1}\ s^{-1}$ at 4.3 K (carrier concentration of $5.08 \times 10^{12}\ cm^{-2}$) to 1730 $cm^2\ V^{-1}\ s^{-1}$ at 300 K (carrier concentration $3.26 \times 10^{12}\ cm^{-2}$), both values represent higher mobilities than that reported on bilayer exfoliated flakes with similar carrier concentration and smaller sample size. This work opens the way for using bilayer graphene on a large scale and overcomes the obstacles imposed by graphene growth on conventional substrates or by using small exfoliated samples.

■ ASSOCIATED CONTENT

Supporting Information

A detailed description of the fabrication steps and growth methods. This material is available free of charge via the Internet at http://pubs.acs.org.

■ AUTHOR INFORMATION

Corresponding Author

*E-mail: luke.nyakiti.ctr@nrl.navy.mil.

■ ACKNOWLEDGMENTS

L.O.N., V.D.W., and F.J.B. acknowledge the support of the American Society for Engineering Education/Naval Research Laboratory Postdoctoral Fellow program. B.R.M. also acknowledges the support from National Research Council. Work at the U.S. Naval Research Laboratory is supported by the Office of Naval Research.

■ REFERENCES

(1) Berger, C.; Song, Z.; Li, T.; Li, X.; Ogbazghi, A. Y.; Feng, R.; Dai, Z.; Marchenkov, A. N.; Conrad, E. H.; First, P. N.; De Heer, W. A. *J. Phys. Chem. B* **2004**, *108* (52), 19912−19916.

(2) De Heer, W. A.; Berger, C.; Wu, X.; P. First, N.; Conrad, E. H.; Li, X.; Lia, T.; Sprinkle, M.; Hass, J.; Sadowski, M. L.; Potemski, M.; Martinez, G. *Solid State Commun.* **2007**, *143* (1−2), 92−100.

(3) Moon, J S.; Curtis, D.; Bui, S.; Hu, M.; Gaskill, D. K.; J Tedesco, L.; Asbeck, P.; Jernigan, G. G.; VanMil, B. L.; Myers-Ward, R. L.; Eddy, C. R. Jr.; Campbell, P. M.; Weng, X. *IEEE Electron Device Lett.* **2010**, *31* (4), 260−262.

(4) Robinson, A J.; Hollander, M.; LaBella, M. III.; Trumbull, K. A.; Cavalero, R.; Snyder, W. D. *Nano Lett.* **2011**, *11* (9), 3875−3880.

(5) Rutter, G. M.; Guisinger, N. P.; Crain, J. N.; First, P. N.; Stroscio, J. A. *Phys. Rev. B* **2010**, *81* (24), 245408.

(6) Seyller, T.; Emtsev, K. V.; Gao, K.; Speck, F.; Ley, L.; Tadich, A.; Broekman, L.; Riley, J. D.; Leckey, R. C. G.; Rader, O.; Varykhalov, A.; A Shikin, M. *Surf. Sci.* **2006**, *600* (18), 3906−3911.

(7) Emtsev, K. V.; Bostwick, A.; Horn, K.; Jobst, J.; Kellogg, G. L.; Ley, L.; McChesney, J. L.; Ohta, T.; Reshanov, S. A.; Röhrl, J.; Rotenberg, E.; Schmid, A. K.; Waldmann, D.; Weber, H. B.; Seyller, T. *Nat. Mater. Lett.* **2009**, *8*, 203−207.

(8) VanMil, B. L.; Myers-Ward, R. L.; Tedesco, J. L.; Eddy, C. R. Jr.; Jernigan, G. G.; Culbertson, J. C.; Campbell, P. M.; McCrate, J. M.; Kitt, S. A.; Gaskill, D. K. *Mater. Sci. Forum* **2009**, *615−617*, 211.

(9) Tedesco, J. L.; VanMil, B. L.; Myers-Ward, R. L.; Culbertson, J. C.; Jernigan, G. G.; Campbell, P. M; McCrate, J. M.; Kitt, S. A.; Eddy, C. R. Jr.; Gaskill, D. K. *ECS Trans.* **2009**, *19*, 137.

(10) Robinson, J. A.; Wetherington, M.; Tedesco, J. L.; Campbell, P. M.; Weng, X.; Stitt, J.; Fanton, M. A.; Frantz, E.; Snyder, D.; Vanmil, B. L.; Jernigan, G. G.; Myers-Ward, R. L.; Eddy, C. R. Jr.; Gaskill, D. K. *Nano Lett.* **2009**, *9* (8), 2873−2876.

(11) Ohta, T.; Bostwick, A.; Seyller, Th.; Horn, K.; Rotenberg, E. *Science* **2006**, *313* (5789), 951−954.

(12) Bolen, M. L.; Harrison, S. E.; Biedermann, L. B.; Capano, M. A. *Phys. Rev. B* **2009**, *80*, 115433.

(13) Orlita, M.; Faugeras, C.; Plochocka, P.; Neugebauer, P.; Martinez, G.; Maude, D. K.; Barra, A.-L.; Sprinkle, M.; Berger, C.; De Heer, W. A.; Potemski, M. *Phys. Rev. Lett.* **2008**, *101* (26), 267601.

(14) Lin, Y.-M.; Farmer, D. B.; Jenkins, K. A.; Wu, Y.; Tedesco, J. L.; Myers-Ward, R. L.; Eddy, C. R.; Gaskill, D. K.; Dimitrakopoulos, C.; Avouris, P. *IEEE Electron Device Lett.* **2011**, *32*, 1343−1345.

(15) Kong, H. S.; Glass, J. T.; Davis, R. F. *J. Appl. Phys.* **1988**, *64* (5), 2672−2679.

(16) Ohtani, N.; Katsuno, M.; Aigo, T.; Fujimoto, T.; Tsuge, H.; Yashiro, H.; Kanaya, M. *J. Cryst. Growth* **2000**, *210* (4), 613−622.

(17) Yakes, M. K.; Gunlycke, D.; Tedesco, J. L.; Campbell, P. M.; Myers-Ward, R. L.; Eddy, C. R. D. Jr.; Gaskill, K.; Sheehan, P. E.; Laracuente, A. R. *Nano Lett.* **2010**, *10* (5), 1559−1562.

(18) Zhang, Y.; Tang, T. T.; Girit, C.; Hao, Z.; Martin, M. C.; Zettl, A.; Crommie, M. F.; Shen, Y. R.; Wang, F. *Nature* **2009**, *459*, 820−823.

(19) Eduardo, V.; Castro, E, V.; Novoselov, K. S.; Morozov, S. V.; Peres, N. M. R.; Lopes dos Santos, J. M. B.; Nilsson, J.; Guinea, F.; Geim, A. K.; Castro Neto, A. H. *Phys. Rev. Lett.* **2007**, *99*, 216802−216804.

(20) Lu, C. L.; Chang, C. P.; Huang, Y. C.; Chen, R. B.; Lin, M. L. *Phys. Rev. B* **2006**, *73*, 144427.

(21) McCann, E. *Phys. Rev. B* **2006**, *74*, 161403.

(22) Neudeck, P. G.; Trunek, A. J.; Spry, D. J.; Powell, J. A.; Du, H.; Skowronski, M.; Huang, X. R.; Dudley, M. *Chem. Vap. Deposition* **2006**, *12* (8−9), 531−540.

(23) Neudeck, P. G.; Du, H.; Skowroronski, M.; Spry, D. J.; Trunek, A. *J. Phys. D: Appl. Phys.* **2007**, *40*, 6139−6149.

(24) Myers-Ward, R. L.; Nyakiti, L. O.; Hite, J. K.; Glembocki, O. J.; Bezares, F. J.; Caldwell, J. D.; Imhoff, G. A.; Hobart, K. D.; Culbertson, J. C.; Picard, Y. N.; Wheeler, V. D.; Eddy, C. R. Jr.; Gaskill, D. K. *Mater. Sci. Forum* **2011**, *679−680*, 119.

(25) Chen, Y.; Kimoto, T.; Takeuchi, Y.; Matsunami, H. *J. Cryst. Growth* **2003**, *254*, 115−122.

(26) Wu, P.; Yoganathan, M.; Zwieback, I. *J. Cryst. Growth* **2008**, *310*, 1804−1809.

(27) Emtsev, K. V.; Bostwick, A.; Horn, K.; Jobst, J.; Kellog, G. L.; Ley, L.; McChesney, J. L.; Ohta, T.; Reshanov, S. A.; Rohrl, J.; Rotenberg, E.; Schmid, A. K.; Waldman, D.; Weber, H. B.; Seyller, T. *Nat. Mater.* **2009**, *8* (3), 203.

(28) Twigg, M. E.; Picard, Y. N. *J. Appl. Phys.* **2009**, *105*, 093520.

(29) Robinson, J.; Weng, X.; Trumbull, K.; Cavalero, R.; Wetherington, M.; Frantz, E.; LaBella, M.; Hughes, Z.; Fanton, M.; Snyder, D *ACS Nano* **2010**, *4* (1), 153−158.

(30) Mohiuddin, T.; Lombardo, A.; Nair, R.; Bonetti, A.; Savini, G.; Jalil, R.; Bonini, N.; Basko, D.; Galiotis, C; Marzari, N.; Novoselov, K. S.; Geim, A.; Ferrari, A. *Phys. Rev. B* **2009**, *79* (20), 205433.

(31) Calizo, I.; Balandin, A.; Bao, W.; Miao, F.; Lau, C. *Nano Lett.* **2007**, *7* (9), 2645−2649.

(32) Eddy, C. R. Jr.; Gaskill, D. K. *Science* **2009**, *324* (5933), 1398−1400.

(33) Ferrari, A. C.; Meyer, J. C.; Scardaci, V.; Casiraghi, C.; Lazzeri, M.; Mauri, F.; Piscanec, S.; Jiang, D.; Novoselov, K. S.; Roth, S.; Geim, A. K. *Phys. Rev. Lett.* **2006**, *97* (18), 187401.

(34) Siegel, D. A.; Zhou, S. Y.; Gabaly, F.; El.; Schmid, A. K.; McCarty, K. F.; Lanzara, A. *Phys. Rev. B* **2009**, *80* (24), 241407(R).
(35) Robinson, J. A.; Puls, C. P.; Staley, N. E.; Stitt, J. P.; Fanton, M. A.; Emtsev, K. V.; Seyller, T.; Liu, Y. *Nano Lett.* **2009**, *9* (3), 964−968.
(36) Röhrl, J.; Hundhausen, M.; Emtsev, K. V.; Seyller, Th.; Graupner, R.; Ley, L. *Appl. Phys. Lett.* **2008**, *92* (20), 201918.
(37) Lespade, P.; Marchand, A.; Couzi, M.; Cruege, F. *Carbon* **1984**, *22*, 375.
(38) Ferrari, A; Robertson, J. *Phys. Rev. B* **2000**, *61*, 14095.
(39) Malard, L. M.; Pimenta, M. A.; Dresselhaus, G.; Dresselhaus, M. S. *Phys. Rep.* **2009**, *473*, 51−87.
(40) Graf, D.; Molitor, F.; Ensslin, K.; Stampfer, C.; Jungen, A.; Hierold, C.; Wirtz, L. *Nano Lett.* **2007**, *7* (2), 238−242.
(41) Das Sarma, S.; Adam, S.; Hwang, E. H.; Rossi, E. *Rev. Mod. Phys.* **2011**, *83*, 407−470.
(42) Ohta, T.; Bartelt, N. C.; Nie, S.; Thürmer, K.; Kellogg, G. L. *Phys. Rev. B* **2010**, *81*, 121411(R).
(43) Malard, M.; Pimenta, M.; Dresselhaus, G.; Dresselhaus, M. *Phys. Rep.* **2009**, *473*, 51−87.
(44) Ni, Z.; Yu, T.; Lu, Y.; Wang, Y.; Feng, Y.; Shen, Z. *ACS Nano* **2008**, *2* (11), 2301−2305.
(45) Hass, J.; Varchon, F.; Millan-Otoya, J. E.; Sprinkle, M.; Sharma, N.; De Heer, W.; Berger, A. C.; First, P. N.; Magaud, L.; Conrad, E. H. *Phy. Rev. Lett.* **2008**, *100* (12), 125504.
(46) Krishnan, K. S.; Ganguli, N. *Nature* **1939**, *144*, 667−667.
(47) Zhu, W.; Perebeinos, V.; Freitag, M.; Avouris, P. *Phys. Rev.* **2009**, *B 80*, 235402.